1/*f* Noise Scaling Analysis in Unipolar-Type Organic Nanocomposite Resistive Memory

Younggul Song,[†] Hyunhak Jeong,[†] Jingon Jang,[†] Tae-Young Kim,[†] Daekyoung Yoo,[†] Youngrok Kim,[†] Heejun Jeong,[*,‡] and Takhee Lee[*,†]

[†]Department of Physics and Astronomy, and Institute of Applied Physics, Seoul National University, Seoul 151-747, Korea and [‡]Department of Applied Physics, Hanyang University, Ansan 426-791, Korea

ABSTRACT

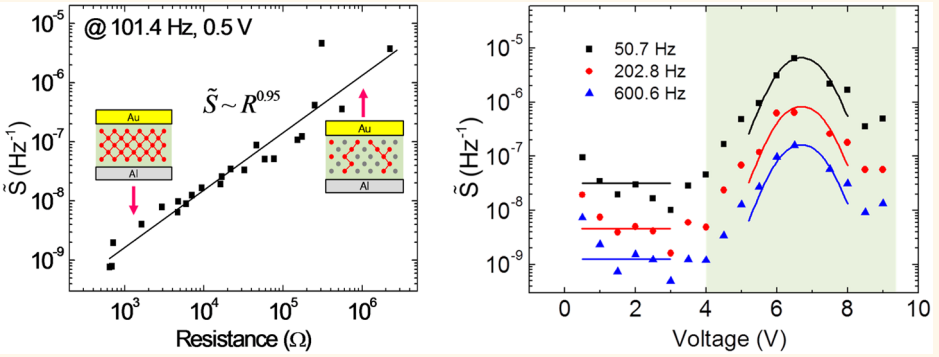

We studied noise characteristics of a nanocomposite of polyimide (PI) and phenyl-C61-butyric acid methyl ester (PCBM) (denoted as PI:PCBM), a composite for the organic nonvolatile resistive memory material. The current fluctuations were investigated over a bias range that covers various intermediate resistive states and negative differential resistance (NDR) in organic nanocomposite unipolar resistive memory devices. From the analysis of the $1/f^{\gamma}$ type noises, scaling behavior between the relative noise power spectral density $\tilde{S}$ and resistance R was observed, indicating a percolating behavior. Considering a linear rate equation of the charge trapping–detrapping at traps, the percolation behavior and NDR could be understood by the modulation of the conductive phase fraction φ with an external bias. This study can enhance the understanding of the NDR phenomena in organic nanocomposite unipolar resistive memory devices in terms of the current path formation and the memory switching.

KEYWORDS: organic nanocomposite · organic memory · unipolar resistive memory · noise characterization · percolation

Organic material-based electronic devices have recently taken significant attention for their various advantages, including low manufacturing cost, large area processing capabilities, flexibility, and printing processes.[1−3] Especially, organic resistive memory devices, in which active polymer materials possess at least two stable resistance states, have been extensively studied for their promising potential for use in storage media.[4−6] Many studies on organic memory have focused on scientific and technical issues of the materials, device structures, switching mechanisms, and performance enhancement.[5−9] However, because of the strongly disordered polymer structures, a consensus on the mechanisms of organic resistive memory has not been achieved.

In particular, the charge conduction in organic memory materials is greatly influenced by the traps that are present in the bulk of the organic memory material or at the interface near the electrodes. In addition, bistable switching can occur from the accumulation of trapped charges, which affect the injection of charges into the organic material and often produce a negative differential resistance (NDR) region in the current–voltage characteristics.[8,10,11] The NDR has been frequently observed in unipolar-type resistive memory from various nanocomposite systems, in which inorganic or organic nanosized particles are

* Address correspondence to hjeong@hanyang.ac.kr, tlee@snu.ac.kr.

Received for review May 26, 2015 and accepted June 30, 2015.

Published online June 30, 2015
10.1021/acsnano.5b03168

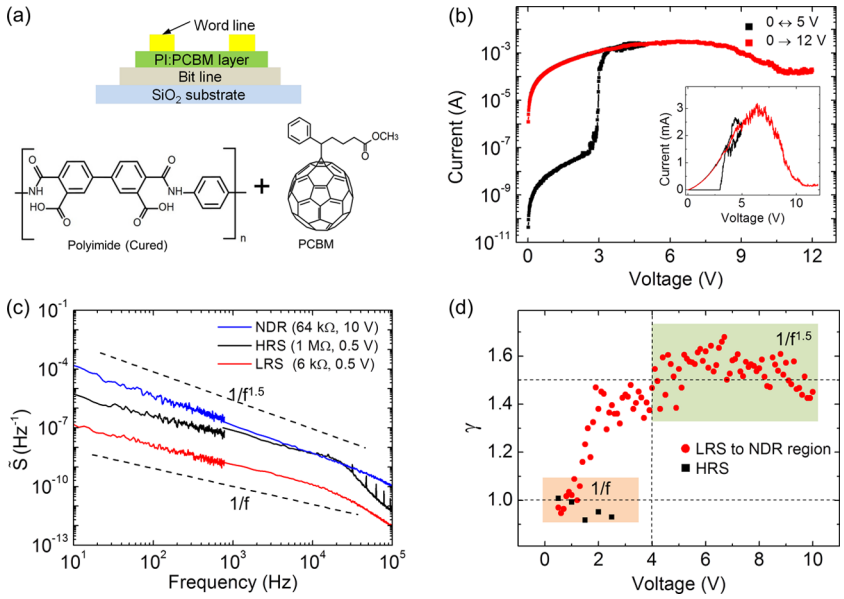

Figure 1. (a) Molecular structures of PI and PCBM. (b) Bistable *I*–*V* characteristics of a PI:PCBM device plotted on a semilogarithmic scale and on a linear scale (inset). (c) Relative power spectrum current noise of LRS, HRS, and NDR. (d) The value of the γ as a function of applied voltage bias in the LRS, HRS, and NDR.

embedded in an insulating matrix.[8,11−13] Some groups explained the NDR phenomenon as the formation and rupture of conducting filaments in organic or inorganic oxide materials under an applied bias.[14,15] Other groups explained the NDR phenomenon as trapping or detrapping of charges at trap.[8,13] However, the switching mechanism for the organic nanocomposite system is still under debate, and few studies have focused on and elaborated the NDR and its derivative intermediate resistive states.

The existing low-frequency noise (LFN) studies provided deep insights into the inherent charge transport mechanisms of various disordered systems, *e.g.*, organic semiconductor,[16] metal−molecule−metal junction,[17,18] inorganic filamentary memory,[14] and granular systems.[19] With an external electric field, the noise data could provide information regarding charge trapping−detrapping phenomena and the percolating behavior of the conduction pathways through the media with randomly distributed trap sites. In this study, we investigated the LFN characteristics of a composite of polyimide (PI) and phenyl-C61-butyric acid methyl ester (PCBM), focusing on the NDR and the multilevel resistive states. The current noise was investigated in both time and frequency domains. We observed that the current noise power spectral density exhibited $1/f^{\gamma}$ noise characteristics, where γ is ∼1 at low bias and ∼1.5 for high bias in the NDR region. In addition, the 1/*f* noise at low bias increased with a power-law scaling as the resistance of the nanocomposite increased, indicating a percolating behavior. We related the conductive phase fraction represented by the ratio of the charge-occupied trap density to the total trap density with the applied bias regarding the charge trapping−detrapping in the NDR region. The percolating behavior and NDR in the nanocomposite memory devices were explained as the modulation of the conductive phase fraction with applied field in the NDR.

RESULTS AND DISCUSSION

A nanocomposite organic material of PI:PCBM (Figure 1a) was used as an active material in the resistive memory device structure. In PI:PCBM nanocomposites, PCBM clusters as electron acceptors are wrapped by a PI insulating matrix. PI:PCBM has been demonstrated to be a promising candidate for the organic nonvolatile resistive memory material due to its stable electrical bistability.[20−22] With a two-terminal device configuration, a PI:PCBM nanocomposite was found to exhibit unipolar switching behavior with a change of resistance, in which the same voltage polarity is used to write and erase the memory states.[20−22] Figure 1b displays the typical current−voltage (*I*–*V*) characteristics of a PI:PCBM memory device on a semilogarithmic current scale. The inset plot in Figure 1b shows the same *I*–*V* data on a linear current scale. Initially, the PI:PCBM is in a high-resistance state (HRS, >1 MΩ). When the applied bias is swept from 0 to 5 V, the PI:PCBM underwent resistive switching, in which the HRS became the low-resistance state (LRS, <10 kΩ). When we swept the bias back to 0 V, the LRS was maintained, exhibiting a high current level. The LRS exhibited Poole−Frenkel conduction behavior (see Figure S1 in the Supporting Information), not an ohmic conduction that has been frequently reported for filamentary conductive resistive memories. The Poole−Frenkel conduction indicates that charge conduction between trap states in the PI:PCBM layer is the main

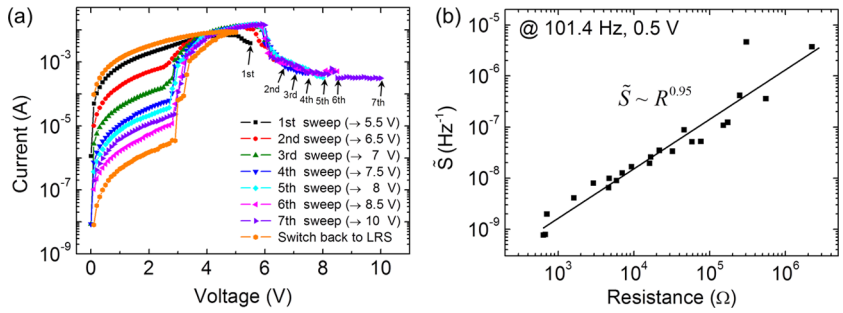

Figure 2. (a) *I*−*V* characteristics of PI:PCBM exhibiting IRSs. (b) Power-law relationship between the relative current noise power spectral density $\tilde{S}$ and the resistance *R* of the IRSs, with *f* = 101.4 Hz and 0.5 V.

conduction mechanism.[23] While sweeping the bias from 0 to 12 V, the NDR was observed from approximately 4 V with unstable and noisy current behavior. When applying a bias over 10 V, the PI:PCBM switched back to the HRS. It is widely accepted that, in the case of nanocomposite organic nonvolatile resistive memory devices, trapping−detrapping of charge carriers occurs at the nanoclusters embedded in the organic insulating matrix.[7,24,25]

Figure 1c shows the relative current noise power spectral density ($\tilde{S} = S_I/I^2$) of the LRS, HRS, and NDR measured for a PI:PCBM memory device. The noise characteristics of the HRS and the LRS were measured at a read voltage of 0.5 V, and those for the NDR were measured at 10 V. Clear 1/*f* noise characteristics were observed in both the HRS and LRS in the frequency range between 10 and 10^4 Hz, with the noise level of the HRS being 2−3 orders of magnitude higher than that of the LRS. The roll-off behavior at $f > 10^4$ Hz is attributed to inevitable capacitive coupling.[16] Unlike the LRS and the HRS, in the NDR region, $1/f^{1.5}$ noise characteristics were observed. This result suggests that the main noise source in the NDR region is different from that of the HRS or LRS. Figure 1d summarizes the exponent γ of the $1/f^{\gamma}$ signal characteristics for the LRS, HRS, and NDR cases, measured from 0.5 to 10 V. In the HRS, the memory device exhibited 1/*f* noise consistently by showing an exponent of $0.9 < \gamma < 1$ until the device was switched to the LRS. In the LRS, the device showed 1/*f* noise behavior when the applied bias was less than 1 V. When the applied bias was over 1 V, the exponent γ gradually increased, and it remained in the range of $1.4 < \gamma < 1.6$ when the bias was greater than 4 V. The increase of the exponent from the LRS to the NDR can be attributed to the onset of trapping−detrapping of charges in deep trap levels.[26,27] We will further discuss this trapping−detrapping behavior later.

Various resistive memory devices based on oxide insulators or nanocomposites, including PI:PCBM, often exhibit intermediate-resistance states (IRSs).[11,14,20] Usually, IRSs can be approached by setting a compliance current or modulating the voltage at which the device is switched off. The PI:PCBM has IRSs of the latter case, which means that modification of the voltage sweep end (V_{end}) in the NDR region causes the device to enter into various current states. In this regard, the HRS and the LRS can be understood as the highest and the lowest resistance states among the IRSs, respectively. In Figure 2a, the representative *I*−*V* characteristics of a PI:PCBM memory device exhibiting IRSs are presented. Starting from the LRS, the applied bias sweep was repeatedly performed by changing the value of V_{end} of each sweep. The value of V_{end} is located in the middle of the NDR region, and the larger the value of V_{end}, the lower the current level becomes. Each IRS was stable, as an IRS could maintain its resistivity under the read voltage of 0.5 V during the noise measurements.

The existence of IRSs leads us to the noise characterization of the IRSs regarding each state as a current distribution through the resistance network of a percolation system.[14] In the PI:PCBM nanocomposite system, the trap sites can be considered to be elementary bonds or sites in percolation theory. In percolation theory, it is known that the relationship between the relative current noise power spectral density $\tilde{S}$ and resistance *R* exhibits a scaling behavior in the condition when the conductive phase fraction φ (the physical meaning of this parameter is the portion of the conducting sites in the media) is larger than a critical phase fraction φ_c and this relationship can be written as[28]

$$\tilde{S} = S_I(f)/I^2 = S_R(f)/R^2 \propto R^{\omega} \text{ (at } \varphi > \varphi_c) \quad (1)$$

Here, the meaning of φ_c is that the memory system becomes from insulating to conductive state by forming a conductive percolating network at φ_c.[28] Also it is well-known that inhomogeneous current distribution in percolation system induces higher $\tilde{S}$.[14,28] As a PI:PCBM device can reach intermediate resistive states, we could obtain $\tilde{S}$ and *R* for a number of resistance values in IRSs. In addition, these IRSs exhibit 1/*f* noise at 0.5 V, as in the cases of the LRS and the HRS. In Figure 2b, the power law relationship between $\tilde{S}$ and *R* of IRSs is shown. Each resistance state is obtained by modification of the value of V_{end} in the NDR region. Because the resistance fluctuation in the NDR is large, even for the same V_{end}, slightly different resistance

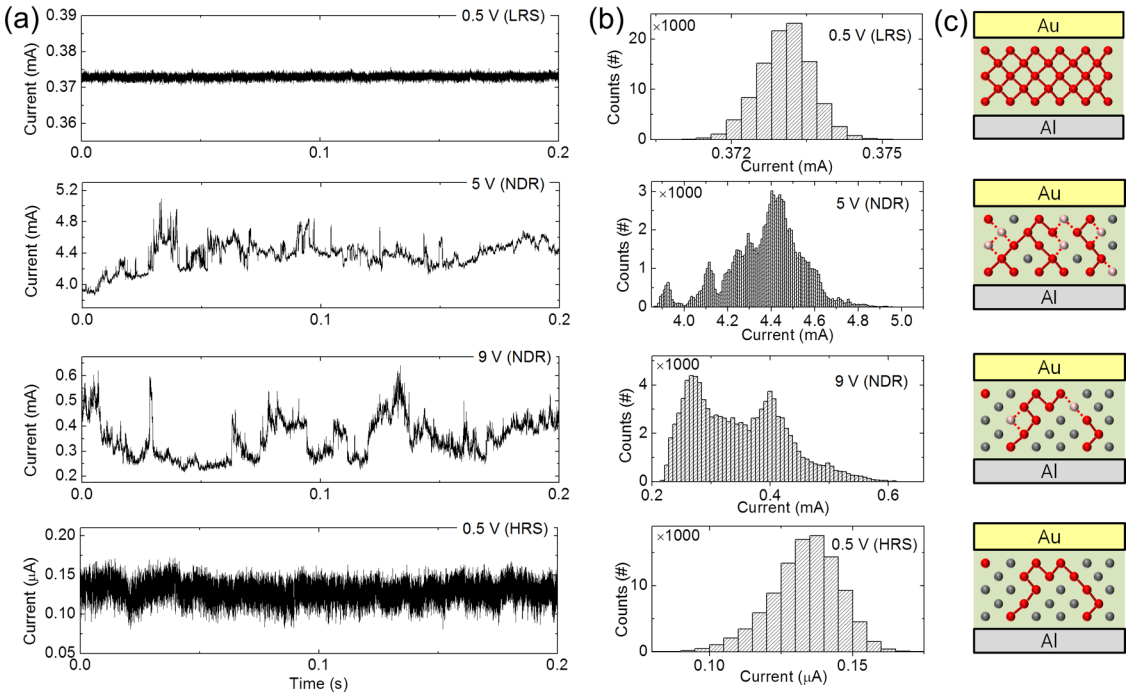

Figure 3. (a) The time trace of currents and (b) the corresponding current histograms for a sequence of applying biases of 0.5, 5, 9, and 0.5 V. (c) Schematics explaining the behaviors of each time-dependent current fluctuation. Gray, red, and pink circles represent the unoccupied traps, occupied traps, and unstable traps in which charge trapping−detrapping occur repeatedly, respectively. The red lines represent the current paths formed between occupied traps. The dashed red lines represent the fluctuating current paths due to unstable traps.

states could be approached. However, the tendency that higher V_{end} leads to a higher resistive state was maintained. We found that the magnitude of $\tilde{S}$ *versus* the resistance of the IRSs exhibited a power law behavior as $\omega = 0.95$ in eq 1, which was consistently observed with the other PI:PCBM memory device studied (see Figure S3 in the Supporting Information). A similar scaling behavior has been observed in various composite systems. For example, values of ω equal to 1.16, 1, and 0.77 were reported for composite systems of PANI:PMMA,[29] AgPt:tetrafluoroethylene,[30] and carbon black:polymer,[31] respectively, in which the scaling behavior was confirmed by varying the ratio of the conducting particles to the embedding insulating matrix. Note that a scaling behavior but with a different power exponent of $\omega = 1.8$ has been reported for a filamentary-type switching NiO resistive memory characterized at room temperature.[14]

The current fluctuations in the time domain were measured. In Figure 3a, current traces were recorded over 0.2 s at room temperature with applied biases in sequence and each data point was acquired with a time interval of 2 μs. The corresponding histograms of the current traces are plotted in Figure 3b. Figure 3c shows the schematics explaining the behaviors of the time-dependent current fluctuation at each bias condition. First, we biased a PI:PCBM device in the LRS with 0.5 V. The device exhibited a simple Gaussian distribution of time-dependent current fluctuation. The distribution of current values has a single peak at the average current value (top figure in Figure 3b). However, when we biased the device in the NDR with 5 and 9 V, the device exhibited abrupt alterations of current values. At 5 V bias in the NDR, at least five peaks were observed in the current histogram; in comparison, two distinct peaks were observed in the current histogram for the case of 9 V bias in the NDR (middle two figures in Figure 3b). After the 9 V bias in the NDR, we applied 0.5 V to cause the PI:PCBM to change to the HRS. The device in the HRS also exhibited a Gaussian distribution of current values (bottom figure in Figure 3b) as is the case in the LRS, but the relative standard deviation (RSD, which is given as $\sigma/\mu \times 100\%$, where μ and σ are the average and standard deviation of current level, respectively) value for the HRS (8.88%) was larger than that (0.15%) for the LRS by approximately 2 orders of magnitude. Because RSD can represent the relative noise amplitude, the HRS shows more noisy behavior than LRS does. The alteration of current traces appears as random telegraph noise (RTN), which is generally explained by trapping and detrapping of charge carriers in the deep trap states.[18,32] Thus, we suggest that the current fluctuation in the NDR is related to the removal of the current pathways *via* the detrapping process of deeply trapped charges (Figure 3c). In our discussion, a charge can pass along the charge-occupied traps, while an electron cannot easily pass the unoccupied traps (see Figure S4 in the Supporting Information). In the LRS, most of the deep trap states are occupied, so most of the conduction process

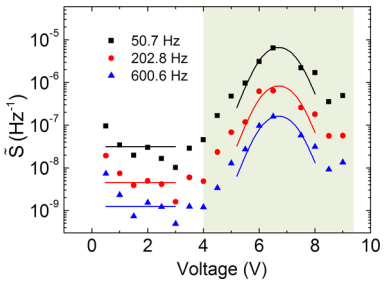

Figure 4. Nonmonotonic behavior between $\tilde{S}$ and the applied bias.

(trapping−detrapping) occurs at shallow trap levels. These trapping−detrapping processes are faster (compared to the ones occurring at the deeper traps) and shallow traps are more uniformly distributed over the material. Therefore, current paths are more numerous and homogeneously distributed, inducing low noise at low bias (top figure in Figure 3c). At higher bias in NDR regime, deeper traps are involved in the conduction process. More deeply trapped charges become unstable and can become detrapped due to the bias-induced lowered trap depth, and the number of current pathways decreases. Thus, the trapping process can occur in the unoccupied trap states, and the trapping−detrapping processes repeat, leading to the fluctuation of number of current pathways (middle two figures in Figure 3c). Deep traps are characterized by longer relaxation times (they are so-called long-lived traps), therefore the noise signal resembles the RTN. With the noise gain due to the fluctuation of number of current pathways, $\tilde{S}$ increases, showing $1/f^{1.5}$ noise behaviors related with RTN-like behavior in NDR regime. When the PI:PCBM is in the HRS by turning off the applied bias, the remaining trapped charges are localized, and the trapping−detrapping process is reduced. At the same time, the current pathways are reduced and their distribution is inhomogeneous, which results in higher RSD in HRS than in LRS (bottom figure in Figure 3c).

We also measured the magnitude of $\tilde{S}$ along the applied bias. In Figure 4, a nonmonotonic behavior between $\tilde{S}$ and applied bias is presented. In the low bias range (0−4 V) in which $1/f$ noise appears, $\tilde{S}$ is almost independent of the applied bias, according to Hooge's empirical relation.[28] On the other hand, in the high bias range (>4 V) in which the NDR begins and $1/f^{1.5}$ noise appears, a noise peak at ∼6 V is observed. This nonmonotonic relationship between $\tilde{S}$ and bias is often explained by the charge trapping−detrapping process at the trap states.[16,18,33]

The scaling behavior between $\tilde{S}$ and R caused by tuning in the NDR can be explained by the detrapping of charge carriers from deep trap sites due to high bias. The PCBM clusters in the PI matrix,[34] the energetic disorder by randomly aligned PI polymers,[35] and penetrated aluminum oxide[11] can be attributed to the deep trap formation. Simplifying the dynamics of charge trapping and detrapping, we can express the rate equation for charge trapping−detrapping as following first-order kinetics, which can be written as[36]

$$\frac{dn^*}{dt} = K_c(n - n^*) - K_t \exp\left[\frac{-\{E_t - E(V_{app})\}}{k_B T}\right] n^* \quad (2)$$

where E_t is the trap depth measured from the conduction-band edge at zero bias. The trap depth can be varied with PCBM cluster size and local disorder of the PI matrix. We assumed that E_t has a continuous and finite range, such as $E_1 < E_t < E_2$ (here, E_1 and E_2 are the lowest and highest energies of the trap depth, respectively), while $n^*\, dE_t$ and $n\, dE_t$ are the densities of filled traps and all the trap sites, respectively, which cover the energy range of $(E_t, E_t + dE_t)$. The first term on the right-hand side of eq 2 is the capture rate of the charges to the unoccupied trap sites from the conduction band. For simplicity, the trapping coefficient (K_c) is considered to be constant because the applied bias in the NDR has a range far beyond the trapping voltage (∼2.5 V). The second term on the right-hand side of eq 2 is the detrapping rate of the electrons from the occupied trap sites *via* thermal excitation. The detrapping coefficient is exponentially dependent on $E_t - E(V_{app})$, which is the effective energy depth of the deep traps with applied bias (V_{app}). Because a higher value of V_{app} will lower the effective energy depth of traps, $E(V_{app})$ is regarded as a monotonically increasing function with V_{app}. When we apply bias in the NDR region for a sufficient time to reach a steady state, n^* can be expressed as $n^* = n/\{1 + (K_t/K_c)\exp[(-E_t + E(V_{app}))/k_B T]\}$, which is a decreasing function of increasing applied bias. Here, we can consider the ratio of all the filled traps to all the traps as the conductive phase fraction φ. Assuming that $n\, dE_t$ is uniform in the range of $E_1 < E_t < E_2$, φ can be written as

$$\varphi = \frac{N^*}{N} = \frac{\int_{E_1}^{E_2} n^*\, dE_t}{\int_{E_1}^{E_2} n\, dE_t}$$

$$= \frac{k_B T}{E_2 - E_1} \mathrm{Log}\left[\frac{e^{E_2/k_B T} + \frac{K_t}{K_c} e^{E(V_{app})/k_B T}}{e^{E_1/k_B T} + \frac{K_t}{K_c} e^{E(V_{app})/k_B T}}\right] \quad (3)$$

Here, N^* and N denote the total density of filled traps and trap sites, respectively. In eq 3, φ is a decreasing function, with values in the range between 1 and 0, with increasing V_{app}. Additionally, the variance of the total number of filled traps is known to be $\Delta N^2 = n_t\varphi(1 - \varphi)$; thus, the $\tilde{S}$ in the NDR region can be expressed as $\tilde{S} \propto \varphi(1 - \varphi)/f^{1.5}$.[33] Consequently, when the applied bias reaches a certain voltage where the conductive phase fraction becomes about 1/2, $\tilde{S}$ reaches the maximum value. After determining the

functional form of $E(V_{app})$ and the ratio between K_c and K_t (see the Supporting Information), we fitted the quadratic relation between $\tilde{S}$ and φ to the NDR region (shaded color) in Figure 4. The fitted curve well explains the peak behavior, with values of E_1 and E_2 of 2.07 and 2.23 eV, respectively, from the fitted curve. This range of trap energy levels is compatible with the trap energy levels induced by impurities in organic polymers.[37]

CONCLUSION

In summary, we performed a systematic investigation into the $1/f^{\gamma}$ noise data of PI:PCBM organic nanocomposite memory devices at various biases including within the NDR region. Our data suggest that intermediate resistance switching effects can be of percolative origin, *i.e.*, the modulation of the current distribution *via* trapping−detrapping processes at deep traps. Using a rate equation based on a charge trapping−detrapping in deep traps, we explained how the applied bias can modulate the conductive phase fraction and lead to percolation behavior in the current noise. This work provides insights into how the NDR phenomena in organic nanocomposite system would actually act on the current path formation and its role in the switching mechanism in unipolar resistive memory devices.

METHODS

For the active nanocomposite organic memory material (PI:PCBM), 2 mL of 3,4,3′,4′-biphenyltetracarboxylic dianhydride-*p*-phenylenediamine (BPDA-PPD) solution (10 wt % in *N*-methyl-2-pyrrolidone(NMP)) as PI precursor and 0.5 mL of PCBM solution (0.5 wt % in NMP) were mixed and then diluted with 11.3 mL of NMP to control the active layer thickness. First, a SiO_2 (270 nm thick)/Si substrate was prepared and cleaned using acetone, 2-propanol, and deionized water for 10 min at each step. The 30 nm-thick Al bottom electrode lines with 100 μm line width were fabricated using a shadow mask patterning. To enhance the film uniformity, the Al bottom electrodes were exposed to UV-ozone for 10 min.[38] The prepared memory solution was spin coated onto the substrate, followed by soft-baking on a hot plate at 120 °C for 5 min and then hard-baking on the hot plate at 300 °C for 30 min in a N_2-filled glovebox. Then, top electrodes of a 30 nm-thick Au layer were deposited on the active memory layer. The PI:PCBM layer thickness was about 20 nm.

The *I*−*V* characteristics of the devices were measured with a semiconductor parameter analyzer (Keithley 4200 SCS) and a probe station system (JANIS Model ST-500). For noise measurement, we used a spectrum analyzer (Stanford Research SR780) and ground-isolated 16-bit analog-digital converter (ADC) to measure low-frequency noise (LFN) on frequency and time domain, respectively. A battery-powered low-noise current amplifier (Ithaco 1211) was used for LFN measurements. A 16-bit digital-analog converter (DAC) was used to apply bias. A digital multimeter (Agilent 34401A) was used to get average electric current coinciding with the noise power spectral density measurement (see Figure S6 in the Supporting Information). All the measurements were performed in vacuum environment and room temperature.

Conflict of Interest: The authors declare no competing financial interest.

Supporting Information Available: Poole−Frenkel conduction at LRS, noise characteristics of PI film, power-law behavior between $\tilde{S}$ and R observed from another device, removal of current pathway with NDR modulation, time traces of three different current level states, details of fitting quadratic relation of $\tilde{S}$ and φ with Figure 4, and noise measurement setup, as well as supplementary figures. The Supporting Information is available free of charge on the ACS Publications website at DOI: 10.1021/acsnano.5b03168.

Acknowledgment. The authors appreciate the financial support of the National Creative Research Laboratory program (Grant No. 2012026372) through the National Research Foundation of Korea (NRF), funded by the Korean Ministry of Science, ICT & Future Planning.

REFERENCES AND NOTES

1. Briseno, A. L.; Mannsfeld, S. C. B.; Ling, M. M.; Liu, S.; Tseng, R. J.; Reese, C.; Roberts, M. E.; Yang, Y.; Wudl, F.; Bao, Z. Patterning Organic Single-Crystal Transistor Arrays. *Nature* **2006**, *444*, 913–917. DOI: 10.1038/nature05427.
2. Rivnay, J.; Jimison, L. H.; Northrup, J. E.; Toney, M. F.; Noriega, R.; Lu, S.; Marks, T. J.; Facchetti, A.; Salleo, A. Large Modulation of Carrier Transport by Grain-Boundary Molecular Packing and Microstructure in Organic Thin Films. *Nat. Mater.* **2009**, *8*, 952–958. DOI: 10.1038/nmat2570.
3. Zhou, Y.; Fuentes-Hernandez, C.; Shim, J.; Meyer, J.; Giordano, A. J.; Li, H.; Winget, P.; Papadopoulos, T.; Cheun, H.; Kim, J.; et al. A Universal Method to Produce Low-Work Function Electrodes for Organic Electronics. *Science* **2012**, *336*, 327–332. DOI: 10.1126/science.1218829.
4. Ouyang, J.; Chu, C.-W.; Szmanda, C. R.; Ma, L.; Yang, Y. Programmable Polymer Thin Film and Non-Volatile Memory Device. *Nat. Mater.* **2004**, *3*, 918–922. DOI: 10.1038/nmat1269.
5. Scott, J. C.; Bozano, L. D. Nonvolatile Memory Elements Based on Organic Materials. *Adv. Mater.* **2007**, *19*, 1452–1463. DOI: 10.1002/adma.200602564.
6. Cho, B.; Song, S.; Ji, Y.; Kim, T.-W.; Lee, T. Organic Resistive Memory Devices: Performance Enhancement, Integration, and Advanced Architectures. *Adv. Funct. Mater.* **2011**, *21*, 2806–2829. DOI: 10.1002/adfm.201100686.
7. Rozenberg, M. J.; Inoue, I. H.; Sánchez, M. J. Nonvolatile Memory with Multilevel Switching: a Basic Model. *Phys. Rev. Lett.* **2004**, *92*, 178302. DOI: 10.1103/PhysRevLett.92.178302.
8. Bozano, L. D.; Kean, B. W.; Deline, V. R.; Salem, J. R.; Scott, J. C. Mechanism for Bistability in Organic Memory Elements. *Appl. Phys. Lett.* **2004**, *84*, 607–609. DOI: 10.1063/1.1643547.
9. Asadi, K.; de Leeuw, D. M.; de Boer, B.; Blom, P. W. M. Organic Non-Volatile Memories from Ferroelectric Phase-Separated Blends. *Nat. Mater.* **2008**, *7*, 547–550. DOI: 10.1038/nmat2207.
10. Tang, W.; Shi, H.; Xu, G.; Ong, B. S.; Popovic, Z. D.; Deng, J.; Zhao, J.; Rao, G. Memory Effect and Negative Differential Resistance by Electrode-Induced Two-Dimensional Single-Electron Tunneling in Molecular and Organic Electronic Devices. *Adv. Mater.* **2005**, *17*, 2307–2311. DOI: 10.1002/adma.200500232.
11. Yang, G.; Chen, H.-Y.; Ma, L.; Shao, Y.; Yang, Y. Study of Multi-ON States in Nonvolatile Memory Based on Metal-Insulator-Metal Structure. *Appl. Phys. Lett.* **2009**, *95*, 203506. DOI: 10.1063/1.3263155.
12. Kang, N.-G.; Cho, B.; Kang, B.-G.; Song, S.; Lee, T.; Lee, J.-S. Structural and Electrical Characterization of a Block Copolymer-Based Unipolar Nonvolatile Memory Device. *Adv. Mater.* **2012**, *24*, 385–390. DOI: 10.1002/adma.201103862.
13. Verbakel, F.; Meskers, S. C. J.; Janssen, R. A. J. Electronic Memory Effects in Diodes of Zinc Oxide Nanoparticles in a Matrix of Polystyrene or Poly(3-hexylthiophene). *J. Appl. Phys.* **2007**, *102*, 083701. DOI: 10.1063/1.2794475.
14. Lee, S. B.; Park, S.; Lee, J. S.; Chae, S. C.; Chang, S. H.; Jung, M. H.; Jo, Y.; Kahng, B.; Kang, B. S.; Lee, M.-J.; et al. Large 1/f

Noise of Unipolar Resistance Switching and Its Percolating Nature. *Appl. Phys. Lett.* **2009**, *95*, 122112. DOI: 10.1063/1.3237167.
15. Rocha, P. R. F.; Gomes, H. L.; Vandamme, L. K. J.; Chen, Q.; Kiazadeh, A.; de Leeuw, D. M.; Meskers, S. C. J. Low-Frequency Diffusion Noise in Resistive-Switching Memories Based on Metal-Oxide Polymer Structure. *IEEE Trans. Electron Devices* **2012**, *59*, 2483–2487. DOI: 10.1109/TED.2012.2204059.
16. Carbone, A.; Kotowska, B. K.; Kotowski, D. Space-Charge-Limited Current Fluctuations in Organic Semiconductors. *Phys. Rev. Lett.* **2005**, *95*, 236601. DOI: 10.1103/PhysRevLett.95.236601.
17. Clèment, N.; Pleutin, S.; Seitz, O.; Lenfant, S.; Vuillaume, D. $1/f^{\gamma}$ Tunnel Current Noise through Si-bound Alkyl Monolayers. *Phys. Rev. B: Condens. Matter Mater. Phys.* **2007**, *76*, 205407. DOI: 10.1103/PhysRevB.76.205407.
18. Kim, Y.; Song, H.; Kim, D.; Lee, T.; Jeong, H. Noise Characteristics of Charge Tunneling *via* Localized States in Metal-Molecule-Metal Junctions. *ACS Nano* **2010**, *4*, 4426–4430. DOI: 10.1021/nn100255b.
19. Mantese, J. V.; Webb, W. W. 1/f Noise of Granular Metal-Insulator Composites. *Phys. Rev. Lett.* **1985**, *55*, 2212–2215. DOI: 10.1103/PhysRevLett.55.2212.
20. Cho, B.; Kim, T.-W.; Song, S.; Ji, Y.; Jo, M.; Hwang, H.; Jung, G.-Y.; Lee, T. Rewritable Switching of One Diode-One Resistor Nonvolatile Organic Memory Devices. *Adv. Mater.* **2010**, *22*, 1228–1232. DOI: 10.1002/adma.200903203.
21. Ji, Y.; Cho, B.; Song, S.; Kim, T.-W.; Choe, M.; Kahng, Y. H.; Lee, T. Stable Switching Characteristics of Organic Nonvolatile Memory on a Bent Flexible Substrate. *Adv. Mater.* **2010**, *22*, 3071–3075. DOI: 10.1002/adma.200904441.
22. Song, S.; Cho, B.; Kim, T.-W.; Ji, Y.; Jo, M.; Wang, G.; Choe, M.; Kahng, Y. H.; Hwang, H.; Lee, T. Three-Dimensional Integration of Organic Resistive Memory Devices. *Adv. Mater.* **2010**, *22*, 5048–5052. DOI: 10.1002/adma.201002575.
23. Chen, J.-C.; Liu, C.-L.; Sun, Y.-S.; Tung, S.-H.; Chen, W.-C. Tunable Electrical Memory Characteristics by the Morphology of Self-Assembled Block Copolymers:PCBM Nanocomposite Films. *Soft Matter* **2012**, *8*, 526–535. DOI: 10.1039/C1SM06622F.
24. Kim, T. W.; Yang, Y.; Li, F.; Kwan, W. L. Electrical Memory Devices Based on Inorganic/Organic Nanocomposites. *NPG Asia Mater.* **2012**, *4*, e18. DOI: 10.1038/am.2012.32.
25. Son, D. I.; You, C. H.; Jung, J. H.; Kim, T. W. Carrier Transport Mechanisms of Organic Bistable Devices Fabricated Utilizing Colloidal ZnO Quantum Dot-Polymethylmethacrylate Polymer Nanocomposites. *Appl. Phys. Lett.* **2010**, *97*, 013304. DOI: 10.1063/1.3454774.
26. Lee, J.-K.; Jeong, H. Y.; Cho, I.-T.; Lee, J. Y.; Choi, S.-Y.; Kwon, H.-I.; Lee, J.-H. Conduction and Low-Frequency Noise Analysis in Al/α-TiO_X/Al Bipolar Switching Resistance Random Access Memory Devices. *IEEE Elec. Dev. Lett.* **2010**, *31*, 603–605. DOI: 10.1109/LED.2010.2046010.
27. Vandamme, L. K. J.; Macucci, M. 1/f and RTS Noise in Submicron Devices: Faster is Noisier. *AIP Conf. Proc.* **2005**, *800*, 436–443. DOI: 10.1063/1.2138649.
28. Kogan, S. Noise in Strongly Disordered Conductors. In *Electronic Noise and Fluctuations in Solids*; Cambridge University Press: New York, 1996; pp 190–202.
29. Planès, J.; François, A. Percolation Scaling, Inhomogeneity, and Defects in Polyaniline Blends: A 1/f Noise Diagnosis. *Phys. Rev. B: Condens. Matter Mater. Phys.* **2004**, *70*, 184203. DOI: 10.1103/PhysRevB.70.184203.
30. Rudman, D. A.; Calabrese, J. J.; Garland, J. C. Noise Spectra of 3-Dimensional Random Metal-Insulator Composites. *Phys. Rev. B: Condens. Matter Mater. Phys.* **1986**, *33*, 1456–1459. DOI: 10.1103/PhysRevB.33.1456.
31. Breeze, A. J.; Carter, S. A.; Alers, G. B.; Heaney, M. B. 1/f Noise through the Metal-Nonmetal Transition in Percolating Composites. *Appl. Phys. Lett.* **2000**, *76*, 592–594. DOI: 10.1063/1.125827.
32. de Sousa, R.; Whaley, K. B.; Wilhelm, F. K.; von Delft, J. Ohmic and Step Noise from a Single Trapping Center Hybridized with a Fermi Sea. *Phys. Rev. Lett.* **2005**, *95*, 247006. DOI: 10.1103/PhysRevLett.95.247006.
33. Carbone, A.; Pennetta, C.; Reggiani, L. trapping–detrapping Fluctuations in Organic Space-Charge Layers. *Appl. Phys. Lett.* **2009**, *95*, 233303. DOI: 10.1063/1.3271769.
34. Wu, J.; Ma, L.; Yang, Y. Single-Band Hubbard Model for the Transport Properties in Bistable Organic/Metal Nanoparticle/Organic Devices. *Phys. Rev. B: Condens. Matter Mater. Phys.* **2004**, *69*, 115321. DOI: 10.1103/PhysRevB.69.115321.
35. Graupner, W.; Leditzky, G.; Leising, G.; Scherf, U. Shallow and Deep Traps in Conjugated Polymers of High Intrachain Order. *Phys. Rev. B: Condens. Matter Mater. Phys.* **1996**, *54*, 7610–7613. DOI: 10.1103/PhysRevB.54.7610.
36. Buchanan, D. A.; Fischetti, M. V.; DiMaria, D. J. Coulombic and Neutral Trapping Centers in Silicon Dioxide. *Phys. Rev. B: Condens. Matter Mater. Phys.* **1991**, *43*, 1471–1486. DOI: 10.1103/PhysRevB.43.1471.
37. Meunier, M.; Quirke, N.; Aslanides, A. Molecular Modeling of Electron Traps in Polymer Insulators: Chemical Defects and Impurities. *J. Chem. Phys.* **2001**, *115*, 2876–2881. DOI: 10.1063/1.1385160.
38. Ji, Y.; Zeigler, D. F.; Lee, D. S.; Choi, H.; Jen, A. K.-Y.; Ko, H. C.; Kim, T.-W. Flexible and Twistable Non-Volatile Memory Cell Array with All-Organic One Diode-One Resistor Architecture. *Nat. Commun.* **2013**, *4*, 2707. DOI: 10.1038/ncomms3707.